Jyväskylän yliopiston julkaisuarkisto
Jyväskylä University Digital Archive

UNIVERSITY OF JYVÄSKYLÄ

This is an electronic reprint of the original article.
This reprint *may differ* from the original in pagination and typographic detail.

Author(s): Delion, D. S.; Suhonen, Jouni

Title: Two-neutrino ββ decays and low-lying Gamow-Teller β− strength functions in the mass range A=70–176

Year: 2017

Version:

Please cite the original version:

Delion, D. S., & Suhonen, J. (2017). Two-neutrino ββ decays and low-lying Gamow-Teller β− strength functions in the mass range A=70–176. Physical Review C, 95(3), Article 034330. https://doi.org/10.1103/PhysRevC.95.034330

All material supplied via JYX is protected by copyright and other intellectual property rights, and duplication or sale of all or part of any of the repository collections is not permitted, except that material may be duplicated by you for your research use or educational purposes in electronic or print form. You must obtain permission for any other use. Electronic or print copies may not be offered, whether for sale or otherwise to anyone who is not an authorised user.

Two-neutrino $\beta\beta$ decays and low-lying Gamow-Teller β^- strength functions in the mass range $A = 70$–176

D. S. Delion
"Horia Hulubei" National Institute of Physics and Nuclear Engineering, 30 Reactorului, RO-077125, Bucharest-Măgurele, România;
Academy of Romanian Scientists, 54 Splaiul Independenţei, RO-050094, Bucharest, România;
and Bioterra University, 81 Gârlei, RO-013724, Bucharest, România

J. Suhonen
University of Jyvaskyla, Department of Physics, P.O. Box 35 (YFL), FI-40014, Jyvaskyla, Finland
(Received 24 November 2016; published 31 March 2017)

We apply the proton-neutron deformed quasiparticle random-phase approximation (pn-dQRPA) to describe the low-lying ($E \leqslant 6$ MeV) 1^+ Gamow-Teller (GT) strength functions in odd-odd deformed nuclei which participate as intermediate nuclei in two-neutrino double-β-decay ($2\nu\beta\beta$) transitions within the mass range $A = 70$–176. In deriving equations of motion we use a single-particle basis with projected angular momentum, provided by the diagonalization of a spherical mean field furnished with a quadrupole-quadrupole interaction. The schematic residual Hamiltonian contains pairing and proton-neutron interaction terms in particle-hole (ph) and particle-particle (pp) channels, with constant strengths. By adopting constant particle-hole and particle-particle strengths we are able to describe the positions of the giant GT resonance and the measured half-lives of the $2\nu\beta\beta$ decays over the whole mass range $A = 70$–176. At the same time we obtain a good agreement with the measured low-lying GT β^- strength functions. By using the adopted ph and pp strengths, we predict the half-lives of a number of deformed $2\nu\beta\beta$ emitters and the low-lying GT strength functions of the corresponding odd-odd intermediate nuclei for their possible experimental tests in the future.

DOI: 10.1103/PhysRevC.95.034330

I. INTRODUCTION

One of the important topics in both nuclear physics and particle physics is the investigation of nuclear double-β ($\beta\beta$) decays [1,2]. The neutrinoless mode, $0\nu\beta\beta$ decay, is especially interesting due to its potential to explore physics beyond the standard model, in particular to discover the fundamental nature of the neutrino. The major problem here is to relate the neutrino properties, depending on the nuclear matrix elements (NMEs) and detailed many-body features of nuclei, to neutrino experiments [3]. At present, there are many models that are able to describe double-β decay in medium-heavy and heavy nuclei. For recent reviews and analyses of these models, see Refs. [4–7].

Along the years, numerous nuclear-structure calculations have been devoted to the description of the two-neutrino mode of the $\beta\beta$ decay ($2\nu\beta\beta$ decay). The $2\nu\beta\beta$ decay can be considered as the first testing ground of a nuclear theory with the aim to describe the $0\nu\beta\beta$ mode [3,8]. The $2\nu\beta\beta$ decay proceeds through the 1^+ states of the intermediate odd-odd nucleus and thus can be related to the Gamow-Teller (GT) strength functions. The GT strength functions in the β^- and β^+ directions are quantitative measures of the magnitudes of the NMEs related to the GT transitions to the intermediate virtual states. Hence, comparison of the calculated strength functions with those measured in charge-exchange reactions (CER) helps assess the quality of the adopted nuclear many-body framework. At present, the CER are a standard tool and comprise the isospin-lowering [(p,n) and $(^3\mathrm{He},t)$ reactions in the β^- direction] and the isospin-raising [(n,p) and $(d,^2\mathrm{He})$ reactions in the β^+ direction] [9]. Recently, a lot of effort has been invested in analyzing the $2\nu\beta\beta$ NMEs via CER (see, e.g., Ref. [10–15]).

There are many nuclear many-body schemes aiming at calculating the half-lives of $\beta\beta$ decays of nuclei. In some of these schemes it is possible to address also the GT strength function, relevant to the analysis of the $2\nu\beta\beta$ half-lives. One very popular nuclear-structure model is the proton-neutron interacting boson model, IBA2. In Ref. [16] it has been used to compute $0\nu\beta\beta$ decay rates of many cases of interest for experimental investigation. In these calculations, the closure approximation has been exploited since the IBA2 model cannot calculate the wave functions of the intermediate odd-odd nucleus. On the other hand, an advantage of the model is that it can take into account the deformation of the mother and daughter nuclei of $\beta\beta$ decay. While the $0\nu\beta\beta$-decay rates are calculable in the closure approximation, the $2\nu\beta\beta$-decay rates are not [3]. This is why the IBA2 model is not suited for calculation of NMEs for $2\nu\beta\beta$ decays and the associated GT strength functions of the involved odd-odd intermediate nuclei. Another problem with IBA2 model is that it can only exploit a model space of one major shell, thus leaving out the spin-orbit-partner orbitals in the adjacent major shells, known to be very relevant for GT type of transitions occurring in $2\nu\beta\beta$ decays [17,18].

The IBA2 model is essentially based on the seniority scheme, as also the more microscopic interacting shell model (ISM) [19]. The ISM suffers from similar problems as the IBA2 by using the closure in the $0\nu\beta\beta$-decay calculations and leaving mostly out the spin-orbit-partner orbitals in its one-major-shell approach. However, the ISM can avoid the closure in the $2\nu\beta\beta$-decay calculations since the GT transitions are easier to handle than the higher-multipole transitions of the $0\nu\beta\beta$ decay. Still, calculations of the GT strength functions are challenging and only their very-low-energy tail can be computed due to the

 ©2017 American Physical Society

limitations in the single-particle model space. The ISM cannot access the GT giant-resonance region at all.

The projected Hartree-Fock-Bogolyubov model (PHFB) of Ref. [20] has been used to compute both $2\nu\beta\beta$ and $0\nu\beta\beta$ decay rates for quite some time now. The model is based on a deformed Hartree-Fock-Bogolyubov mean field complemented by a summation method to take into account, in an effective way, the correlations beyond the mean field. However, this model is still basically just a mean-field model that is unable to calculate the wave functions of the intermediate odd-odd nucleus and thus the related GT strength functions.

Another interesting model is the mean-field model [21] based on a Gogny energy-density functional. The sore point of this approach is the same as for IBA2: Both these models have to use closure approximation, thus excluding calculations of $2\nu\beta\beta$ decay rates and GT strength functions.

A further model, designed to calculate GT and other nuclear transitions, is the projected shell model (PSM) [22]. It starts from a deformation-dressed single-particle basis with good spherical quantum numbers. Since the PSM is applied to (axially) deformed nuclei, the effectively deformed single-particle wave functions lead to an efficient handling of nuclear structure and small dimensions of the many-body model space. It is also a multishell model suited to description of, e.g., parity-changing decay operators. As far as we know, its feasibility for calculations of $2\nu\beta\beta$-decay properties has not been tested yet.

The traditionally used microscopic model for double-β calculations is the proton-neutron quasiparticle random-phase approximation (pn-QRPA) [23]. In this approach, all the wave functions of states of the intermediate odd-odd nuclei, in both $2\nu\beta\beta$ and $0\nu\beta\beta$ decays, can be calculated and no closure is forced in the $\beta\beta$-decay calculations. At the same time, the full GT strength function, including the giant-resonance region, of the intermediate nucleus can be accessed without difficulty. Mostly the pn-QRPA based on a spherical mean field has been used in the calculations. However, many β and double-β decaying nuclei are more or less deformed and therefore it is very important to extend the description to a deformed mean field. This is the starting point of the deformed pn-QRPA (pn-dQRPA). Most earlier approaches describe GT β decays by using a pn-dQRPA phonon in the intrinsic system of coordinates, i.e., in terms of pairs of Nilsson quasiparticles coupled to a $K = 1$ spin projection. The physical observables, like β-decay transition probabilities, are then estimated by rotating the intrinsic phonon to the laboratory system of coordinates [24,25]. This formalism was applied in order to describe the 1^+ GT states and $2\nu\beta\beta$ decays in several papers [26–29].

Let us mention that this projection procedure restores only the symmetry of the phonon, by leaving the pn-dQRPA ground state deformed. A more consistent approach is to use a single-particle (sp) basis with good angular momentum, directly in the derivation of the pn-dQRPA equations.

One way to obtain this basis is projecting good angular momentum from the product between a coherent state, describing the deformed core, and a spherical sp state [30]. The pn-dQRPA phonon, describing GT β decays, is built by using pairs of these quasiparticles that are "dressed by deformation," coupled to the spin $J = 1$ [31,32]. In Ref. [33] this approach was generalized, by considering all allowed spherical sp states in order to build a sp state "dressed by deformation." A particular case is the adiabatic limit, which coincides with the usual Nilsson wave function rotated to the laboratory frame. We successfully described the available experimental $B(E2)$ values for collective states in the range $50 \leqslant Z \leqslant 100$ in even-even nuclei, by using the adiabatic version of this formalism [33].

In the present work we use the pn-dQRPA to predict the $2\nu\beta\beta$ half-lives and the low-lying β^- GT strength functions of the involved intermediate odd-odd nuclei for a total of 20 $\beta\beta$ emitters within the mass range $A = 70$–176. The involved nuclei have quadrupole deformations ranging from $\beta = 0.00$ (spherical) to $\beta = 0.28$ (rigid rotor). The deformation plays an important role in quantitative prediction of the $2\nu\beta\beta$ half-lives, in particular through a deformation difference between the mother and daughter nuclei.

II. THEORETICAL BACKGROUND

In order to describe the 1^+ GT states in odd-odd deformed nuclei, we will proceed by using the steps described in Ref. [34].

(1) We first build a deformed sp basis with good angular momentum. To this purpose we use the sp Nilsson representation, but transformed in the laboratory system of coordinates [33]

$$|\tau jm) = a^\dagger_{\tau jm}(\Omega)|0) = \sum_{J=\text{even}} \sum_{j_s \geqslant j} \mathcal{X}^{Jk_s}_{\tau j} [Y_J(\Omega) \otimes |\tau k_s\rangle]_{jm},$$
$$|\tau k_s \nu\rangle = c^\dagger_{\tau k_s \nu}|0\rangle, \quad \tau = p,n. \tag{1}$$

Here, Ω denotes Euler angles of the intrinsic symmetry axis with respect to the laboratory system and $j \equiv (\epsilon, j^\pi)$ (deformed eigenvalue, total spin$^{\text{parity}}$). The creation operators $c^\dagger_{\tau k_s \nu}$ describe the eigenstates of a spherical nuclear plus proton Coulomb mean field having the quantum numbers $k_s \equiv (e,l,j_s)$, (spherical eigenvalue, orbital angular momentum, total spherical spin), with ν being the z projection of j_s. The expansion coefficients are proportional to standard Nilsson amplitudes with $j = K$, where K is the spin projection on the intrinsic symmetry axis

$$\mathcal{X}^{Jk_s}_{\tau j} = \sqrt{2}\langle jj; j_s - j|J0\rangle x^{k_s}_{\tau j}, \tag{2}$$

where by brackets we denoted the Clebsch-Gordan coefficient. The amplitudes $x^{k_s}_{\tau j}$ are found by diagonalizing the quadrupole operator in the spherical Woods-Saxon basis. Let us mention that both amplitudes satisfy orthonormality relations. In the spherical limit, where one has $x^{k_s}_{\tau j} = \delta_{j_s j}$, the operator (1) is proportional to the usual spherical sp creation operator with a "statistical" coefficient

$$\mathcal{X}^{Jk_s}_{\tau j} = \sqrt{\frac{2}{2j+1}}\delta_{j_s j}, \tag{3}$$

expressing the fact that two particles with intrinsic projections $K = \pm j$ are distributed over $2j + 1$ projections in the laboratory system of coordinates.

(2) We transform the one-body operators in this representation, because we use a Hamiltonian with separable forces. For a particle-hole (ph) operator

$$Q_{\lambda\mu} = \sum_{j_1 j_2} \frac{(\tau_1 j_1 || Q_\lambda || \tau_2 j_2)}{\hat{\lambda}} \left[a^\dagger_{\tau_1 j_1} \otimes \tilde{a}_{\tau_2 j_2} \right]_{\lambda\mu}, \quad (4)$$

where for simplicity we dropped the Euler angles Ω, the reduced matrix element in the deformed basis (1) is given by the integration over Euler angles. The result is a superposition of standard spherical reduced matrix elements

$$\begin{aligned}(\tau_1 j_1 || Q_\lambda || \tau_2 j_2) &= \hat{j_1}\hat{j_2} \sum_{J k_{s1} k_{s2}} \mathcal{X}^{J k_{s1}}_{\tau_1 j_1} \mathcal{X}^{J k_{s2}}_{\tau_2 j_2} (-)^{j_{s1}+j_2+\lambda-J} \\ &\times W(j_1 j_{s1} j_2 j_{s2}; J\lambda) \langle \tau_1 k_{s1} || Q_\lambda || \tau_2 k_{s2} \rangle, \quad (5)\end{aligned}$$

where $\hat{j} = \sqrt{2j+1}$ and W is the Racah symbol. Obviously one has a similar result for a particle-particle (pp) operator. For the monopole particle-number and pairing operators in the laboratory system, we will consider the leading $J = 0$ component

$$\begin{aligned}N_{\tau j} &\approx \left(x^j_{\tau j}\right)^2 \frac{2}{2j+1} \sum_m a^\dagger_{\tau j m} a_{\tau j m}, \\ P^\dagger_{\tau j} &\approx \left(x^j_{\tau j}\right)^2 \frac{2}{2j+1} \sum_m a^\dagger_{\tau j m} a^\dagger_{\tau j -m} (-)^{j-m}. \quad (6)\end{aligned}$$

We use a monopole pairing plus a separable proton-neutron interaction, with constant strengths, in both the ph and pp channels

$$\begin{aligned}H &= \sum_p (\epsilon_p - \lambda^{\rm prot}) N_p - \frac{G^{\rm prot}_{\rm pair}}{4} \sum_{pp'} P^\dagger_p P_{p'} \\ &+ \sum_n (\epsilon_n - \lambda^{\rm neut}) N_n - \frac{G^{\rm neut}_{\rm pair}}{4} \sum_{nn'} P^\dagger_n P_{n'} \\ &+ g_{\rm ph} \sum_\mu D^-_{1\mu} (D^-_{1\mu})^\dagger - g_{\rm pp} \sum_\mu P^-_{1\mu} (P^-_{1\mu})^\dagger, \quad (7)\end{aligned}$$

where the meaning of the short-hand notation is $\tau \equiv (\tau, \epsilon j^\pi)$. Here, the chemical potential for protons (neutrons) is denoted by $\lambda^{\rm prot}$ ($\lambda^{\rm neut}$). The strength parameters $g_{\rm ph}$ (particle-hole) and $g_{\rm pp}$ (particle-particle) are the ones of the corresponding spherical limit in Refs. [35,36] and are given in units of MeV.

The GT operators are given by

$$\begin{aligned}D^-_{1\mu} &= \frac{1}{\sqrt{3}} \sum_{pn} (p || \sigma || n) [a^\dagger_p \otimes \tilde{a}_n]_{1\mu}, \\ P^-_{1\mu} &= \frac{1}{\sqrt{3}} \sum_{pn} (p || \sigma || n) [a^\dagger_p \otimes a^\dagger_n]_{1\mu}. \quad (8)\end{aligned}$$

Here, σ_μ is the Pauli operator and the reduced matrix element in the deformed basis (1) is given in terms of the standard spherical matrix element by Eq. (5) with $\lambda = 1$.

(3) We then introduce quasiparticle representation for protons and neutrons via

$$a^\dagger_{\tau m} = u_\tau \alpha^\dagger_{\tau m} + v_\tau \alpha_{\tau -m} (-)^{j_\tau - m}, \quad (9)$$

where u and v are the BCS vacancy and occupation amplitudes, respectively, in order to obtain the β-decay operators entering the Hamiltonian (7). The BCS equations have formally the same form as for the spherical case due to the "statistical" factors, entering the particle-number and pairing operators (6).

(4) Finally we diagonalize the proton-neutron interaction within the pn-dQRPA by using the phonon

$$\Gamma^\dagger_{1\mu}(\omega) = \sum_{pn} \left[X^\omega_{pn} A^\dagger_{1\mu}(pn) - Y^\omega_{pn} (-)^{1-\mu} A_{1-\mu}(pn) \right], \quad (10)$$

where ω is the eigenvalue index, in terms of the creation pair operator

$$A^\dagger_{1\mu}(pn) = [\alpha^\dagger_p \otimes \alpha^\dagger_n]_{1\mu}. \quad (11)$$

The equations of motion are derived by using the projection procedure over the Euler angles, i.e.,

$$\int d\Omega \left\{ A_{1\mu}, \left[H, \Gamma^\dagger_{1\mu}(\omega) \right] \right\} = \omega \int d\Omega \left[A_{1\mu}, \Gamma^\dagger_{1\mu}(\omega) \right], \quad (12)$$

and a similar relation with $A^\dagger_{1-\mu}$. In this way, one obtains the standard pn-dQRPA equations of motion determining the eigenvalues ω and amplitudes X^ω, Y^ω [33,37]. They formally coincide with the spherical pn-QRPA equations, but the pair basis in the phonon (10) couples proton and neutron states with deformed sp spectra. Thus, in the present approach the QRPA vacuum is spherical, in contrast to the approximations adopted earlier where the spherical symmetry of the phonon was restored after deriving the equations of motion, still leaving the vacuum itself deformed.

We will estimate the β^- strength function by using the GT β-decay transition matrix elements [37]

$$\begin{aligned}(\omega || \beta^- || 0) &= \sum_{pn} (p || \sigma || n) \left[u_p v_n X^\omega_{pn} + v_p u_n Y^\omega_{pn} \right], \\ (\omega || \beta^+ || 0) &= \sum_{pn} (p || \sigma || n) \left[v_p u_n X^\omega_{pn} + u_p v_n Y^\omega_{pn} \right]. \quad (13)\end{aligned}$$

The $2\nu\beta\beta$ GT matrix element is written as follows [23]:

$$M_{\rm GT} = \sum_{mn} \frac{\left(0 || \beta^- || \omega^f_m\right) \left\langle \omega^f_m | \omega^i_n \right\rangle \left(\omega^i_n || \beta^- || 0\right)}{D_m}, \quad (14)$$

where the energy denominator is given by

$$D_m = \frac{\frac{1}{2}\left(\Delta_{\rm exp} + \tilde{\omega}^i_m + \tilde{\omega}^f_m\right) + E_{\rm ex}(1^+_1) + \Delta M^{\rm exp}_i}{m_e c^2}. \quad (15)$$

Here, $\tilde{\omega}_m = \omega_m - \omega_1$, $\Delta_{\rm exp}$ is the nuclear mass difference between initial and final states, $E_{\rm ex}(1^+_1)$ is the experimental

energy of the first 1^+ state in the intermediate odd-odd nucleus, $\Delta M_i^{\rm exp}$ is the measured difference of the mass energies of the intermediate and initial nuclei, and $m_e c^2$ is the electron rest mass. Here we use as much as possible experimental information in constructing the energy denominator (15) in order to avoid additional uncertainties rising from the description of nuclear mass differences by the pn-dQRPA formalism. The overlap between the initial 1_n^+ and final 1_m^+ states in (14), $\langle\omega_m^f|\omega_n^i\rangle$, is given by a relation similar to Eq. (29) of Ref. [27], where we use pn-dQRPA amplitudes. This permits the use of a different deformation in the initial and final nucleus of double-β decay.

III. NUMERICAL APPLICATION

We analyzed the β-decay strength function by using our pn-dQRPA formalism. To this purpose we describe the 1^+ states of the odd-odd nucleus by using pn-dQRPA eigenstates. We use as spherical sp states $c^\dagger_{\tau k_s \nu}$ the eigenstates of the Woods-Saxon plus proton Coulomb mean field with the universal parametrization of Ref. [38]. The deformed eigenstates $a^\dagger_{\tau jm}$, given by Eq. (1), are obtained by diagonalizing the quadrupole-quadrupole interaction in the adiabatic limit. The deformation parameters are taken from Ref. [39]. The u and v amplitudes were determined by solving the BCS equations with monopole interaction reproducing the experimental pairing gaps in the initial and final nuclei.

The GT strength of a β^- transition from the 0^+ ground state of the even-even mother nucleus to the 1^+ state ω in the odd-odd daughter nucleus nucleus is given by the square of the corresponding transition amplitude, i.e., by

$$B(\mathrm{GT}^-)(\omega) = [g_{\rm A}(\omega||\beta^-||0)]^2, \tag{16}$$

where $g_{\rm A}$ is the axial-vector coupling constant of the weak current. The GT strength function consists of the strengths (16) as a function of the 1^+ energy $E(\omega)$ in the daughter nucleus, taken relative to the ground state of the daughter (i.e., relative to the 2^- ground state of ^{76}As in the case of the transitions $^{76}\mathrm{Ge} \to {}^{76}\mathrm{As}$). A convenient way to represent the evolution of the GT strength function is to use the cumulative strength defined by

$$S(E) = \sum_{E(\omega)\leqslant E} B(GT^-)(\omega), \tag{17}$$

where the sum runs over all 1^+ states ω with their energies $E(\omega)$ being less or equal to a given energy E. The total GT strength, $B(\mathrm{GT})_{\rm tot}$, is obtained by letting $E \to \infty$. Most of the total strength is gathered by the GT giant resonance (GTGR) located between 10 and 20 MeV in the odd-odd daughter. The corresponding energy $E_{\rm GTGR}$ is obtained as the centroid of energies of the 1^+ states belonging to the GTGR.

In Table I we summarize our results for the centroid $E_{\rm GTGR}$ of the GTGR (column 8) and the total GT strength (last column). These results are compared with the available data in columns 7 and 9, respectively. In Table I we give also the charge and mass number of the parent nucleus (columns 2 and 3), and quadrupole deformations [39] of the $2\nu\beta\beta$ mother (Z,N) and daughter $(Z-2,N+2)$ nuclei (columns 5 and 6). In the calculations we used a common value of the particle-hole strength, $g_{\rm ph} = 0.16$ MeV, in order to reproduce the experimental centroid of the GT β^--type strength $B(\mathrm{GT}^-)$ in the giant-resonance region. For the nuclei ^{76}Ge, ^{128,130}Te, and ^{150}Nd we could use the measured values of $E_{\rm GTGR}$, while for the other $\beta\beta$ emitters we applied the empirical relation of Ref. [37]. We adopted a quenched value of the effective axial-vector coupling $g_{\rm A} = 0.75$ according to the analyses performed in Ref. [40]. This choice of $g_{\rm A}$ value is also consistent with the experimental total GT strength of the same nuclei, as seen by comparison of the numbers in columns 9 and 10.

TABLE I. Charge and mass number of the $2\nu\beta\beta$ parent nucleus, quadrupole deformations [39] of the $2\nu\beta\beta$ mother (Z,N) and daughter $(Z-2,N+2)$ nuclei, experimental and theoretical values of the centroid of the GT giant resonance (relative to the ground state of the odd-odd nucleus), and total GT strength.

n	Parent nucleus			Deformation		$E_{\rm GTGR}$ (MeV)		$B(\mathrm{GT})_{\rm tot}$	
		Z	A	β_i	β_f	Exp	Th	Exp	Th
1	Zn	30	70	0.04	−0.24	11.32	7.51		18.18
2	Ge	32	76	0.15	0.20	11.13	11.56	19.89	21.03
3	Se	34	80	0.15	0.06	10.66	10.44		20.85
4	Se	34	82	0.15	0.07	11.71	11.27		24.01
5	Kr	36	86	0.16	0.05	11.95	10.61		23.87
6	Zr	40	94	0.06	0.05	12.85	12.84		24.22
7	Zr	40	96	0.22	0.08	13.28	13.35		27.36
8	Mo	42	100	0.24	0.16	13.57	12.50		27.45
9	Ru	44	104	0.25	0.16	13.20	12.09		27.51
10	Pd	46	110	0.22	0.14	13.49	13.33		30.80
11	Te	52	128	0.00	0.14	13.14	12.28	40.08	41.14
12	Te	52	130	0.00	−0.11	13.59	12.73	45.90	44.51
13	Xe	54	134	0.00	−0.11	13.51	12.72		44.42
14	Xe	54	136	0.00	0.00	14.22	13.77		47.77
15	Ce	58	142	0.00	0.00	15.04	13.84		44.33
16	Nd	60	148	0.21	0.16	15.43	15.47		47.37
17	Nd	60	150	0.24	0.21	15.00	16.42	47.74	50.69
18	Sm	62	154	0.27	0.24	15.37	16.51		50.67
19	Gd	64	160	0.28	0.27	16.15	16.89		54.03
20	Yb	70	176	0.28	0.28	16.98	18.01		60.77

The position of the centroid $E_{\rm GTGR}$ is insensitive to the value of the $g_{\rm pp}$ strength but the $2\nu\beta\beta$ half-life is very sensitive to this parameter. We computed the $2\nu\beta\beta$ matrix element (14) for a fixed value of the particle-particle strength, $g_{\rm pp} = 0.04$ MeV, and obtained the predicted half-lives in the sixth column of Table II. It is worth noting that the presently adopted values $g_{\rm ph} = 0.16$ MeV and $g_{\rm pp} = 0.04$ MeV are compatible with the ranges of values of the corresponding parameters 2χ and 2κ used in the spherical pnQRPA calculations of the $2\nu\beta\beta$-decay rates, e.g., in Refs. [35,36].

In Table II, column 6, we summarize our results for the $2\nu\beta\beta$ half-life. The computed half-lives are in quite reasonable agreement with the available eight measured half-life values, given in the fifth column. In the seventh column of Table II we give for comparison recent results from a nuclear shell-model calculation [42]. The results of these calculations compare well with our present ones, except for ^{128}Te, where our calculations predict a factor 5 too long a half-life but the shell model seems

TABLE II. Charge and mass number of the $2\nu\beta\beta$ parent nucleus, and experimental and computed $2\nu\beta\beta$ half-lives in units of years.

n		Z	A	Exp. [41]	Th.	Shell model [42]	pnQRPA [43]	pnQRPA [44]
1	Zn	30	70		1.82×10^{24}			$(7.0 \pm 4.1) \times 10^{22}$
2	Ge	32	76	$(1.60^{+0.13}_{-0.10}) \times 10^{21}$	1.05×10^{21}	$(2.1–2.3) \times 10^{21}$		
3	Se	34	80		9.33×10^{29}			$(2.6 \pm 1.7) \times 10^{29}$
4	Se	34	82	$(9.2 \pm 0.7) \times 10^{19}$	5.75×10^{19}	$(5.8–6.0) \times 10^{19}$		
5	Kr	36	86		4.57×10^{23}			
6	Zr	40	94		5.75×10^{22}			
7	Zr	40	96	$(2.3 \pm 0.2) \times 10^{19}$	3.63×10^{19}			
8	Mo	42	100	$(7.1 \pm 0.4) \times 10^{18}$	2.40×10^{19}		4.6×10^{18}	$(1.1 \pm 0.6) \times 10^{19}$
9	Ru	44	104		3.02×10^{22}		4.8×10^{21}	$(7.8 \pm 1.7) \times 10^{21}$
10	Pd	46	110		3.47×10^{20}		2.2×10^{20}	$(1.5 \pm 0.3) \times 10^{20}$
11	Te	52	128	$(2.0 \pm 0.3) \times 10^{24}$	9.77×10^{24}	1.6×10^{24}	2.0×10^{24}	$(0.8 \pm 0.2) \times 10^{24}$
12	Te	52	130	$(6.9 \pm 1.3) \times 10^{20}$	5.50×10^{20}	5.2×10^{20}	3.4×10^{20}	
13	Xe	54	134		4.57×10^{24}		2.2×10^{24}	
14	Xe	54	136	$(2.20 \pm 0.06) \times 10^{21}$	5.01×10^{21}	1.6×10^{21}	$(1.4–2.4) \times 10^{21}$	
15	Ce	58	142		3.80×10^{22}			
16	Nd	60	148		1.23×10^{21}			
17	Nd	60	150	$(8.2 \pm 0.9) \times 10^{18}$	8.13×10^{18}			
18	Sm	62	154		3.89×10^{22}			
19	Gd	64	160		2.95×10^{21}			
20	Yb	70	176		1.29×10^{23}			

to work well. In column 8 we present the results of spherical pnQRPA calculations conducted in Ref. [43]. In the study [43] an extended study of the β^- and β^+/EC decays in the mass range $A = 100$–136 was conducted to gain information on the value of the g_{pp} parameter and g_A in the pnQRPA framework. Although the studies were performed by using the Bonn-A G-matrix-based effective two-body interactions, the obtained (average) value of $g_A = 0.60$ corresponds nicely to the one of the present study. In addition, the gained $2\nu\beta\beta$ half-lives were quite good, though in many cases slightly too short, and shorter than in the present study including the deformation. As seen from Table II, in the cases of notable deformation ($A = 100, 104, 110$) the presently predicted half-lives deviate substantially from those deduced in Ref. [43]. The qualitative features of the $2\nu\beta\beta$ half-lives obtained in Ref. [43] can also be seen in the study [44] in which a more extended global Markov chain Monte Carlo study of the β^- and β^+/EC decays was performed in the spherical pnQRPA framework in order to access the values of g_{pp} and g_A. The derived $2\nu\beta\beta$ half-lives of the study [44] are presented in the last column of Table II and they follow the trends of those obtained in Ref. [43].

In fact, the agreement of the presently computed $2\nu\beta\beta$ half-lives with the experimental ones is better than in our earlier paper [34] where we validated our model by comparison with the experimental Gamow-Teller properties of ^{150}Nd and the $2\nu\beta\beta$ half-lives of seven measured cases. In this study the global optimization of the interaction parameters was not done, which explains the better results of the present calculations. Instead, in Ref. [34] the general properties of nuclei, when going from the spherical regime to the deformed region, were outlined, including discussion of the effects of different deformations in the $2\nu\beta\beta$ parent and daughter nuclei. The main message was that in the $2\nu\beta\beta$ systems both the deformation as such and in particular the difference in deformations reduces the overlap of the intermediate states and thus the $2\nu\beta\beta$ decay probability, exceptions being the (close to) semimagic systems with zero deformation.

It is worth noting that the cumulative strength of (17), $S(E)$, reproduces the order of magnitude of the experimental data in the low-energy part of the spectrum, as seen in Figs. 1 and 2. In these figures we plot by a solid line the computed cumulative strength versus excitation energy for the reference nuclei ^{76}Ge, ^{82}Se, ^{96}Zr, and ^{100}Mo [Figs. 1(a)–1(d), respectively] and for

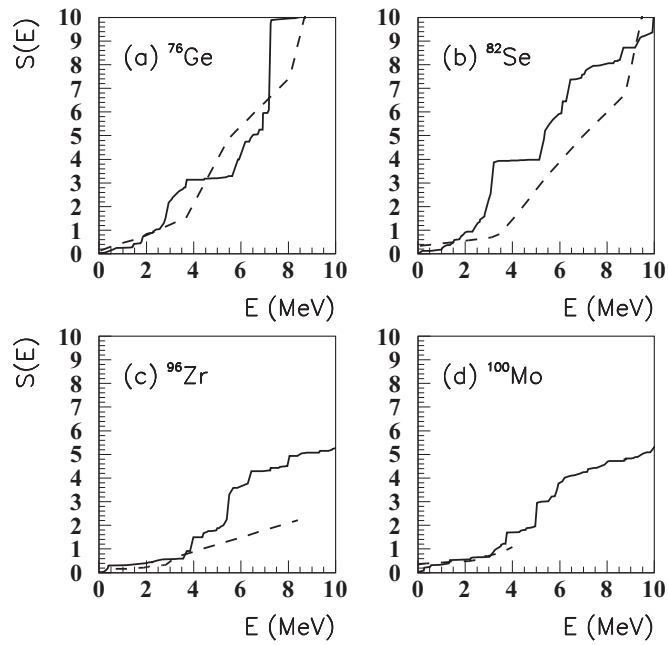

FIG. 1. Computed cumulative GT strength (17) (solid lines) vs experimental values (dashed lines) for ^{76}Ge [12,45] (a), ^{82}Se [45] (b), ^{96}Zr [13] (c), and ^{100}Mo [14] (d). The excitation energy is always relative to the ground state of the odd-odd daughter nucleus.

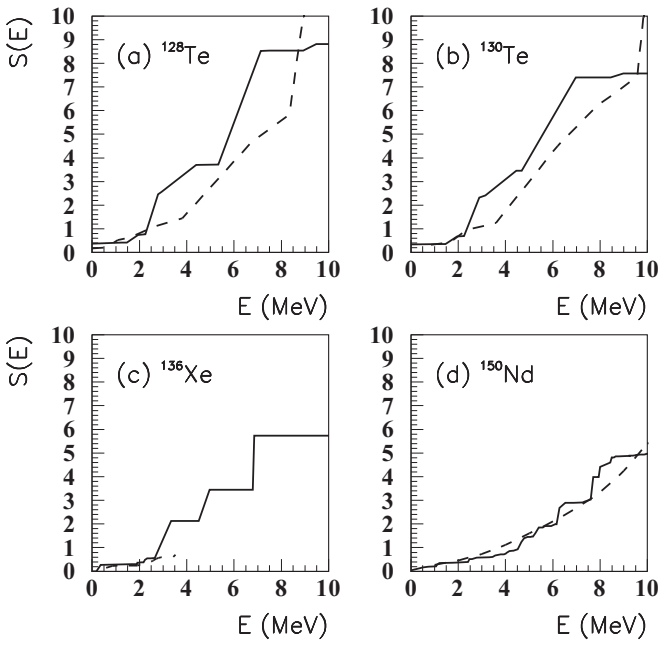

FIG. 2. Same as in Fig. 1 for ^{128}Te [15] (a), ^{130}Te [15] (b), ^{136}Xe [10] (c), and ^{150}Nd [11] (d).

^{128}Te, ^{130}Te, ^{136}Xe, and ^{150}Nd [Figs. 2(a)–2(d), respectively]. The experimental cumulative strength is given by dashed lines in these figures. The experimental cumulative strength is very well reproduced by the calculations for ^{76}Ge [Fig. 1(a)], ^{100}Mo [Fig. 1(d)], ^{136}Xe [Fig. 2(c)], and ^{150}Nd [Fig. 2(d)]. For ^{82}Se [Fig. 1(b)], ^{128}Te [Fig. 2(a)], and ^{130}Te [Fig. 2(b)], there is a bit too much strength at around 3 MeV. For ^{96}Zr [Fig. 1 (c)] the pn-dQRPA predicts too much strength beyond 4 MeV.

The interesting part of Table I are the predicted total GT strengths of column 10 and the predicted $2\nu\beta\beta$ half-lives of the sixth column of Table II. These predictions now await future experimental tests. In addition to Figs. 1 and 2 we give in Table III the low-lying total strength within bins of half an MeV for better comparison with the present and future experimental data.

We summarize the GT strength of Table III in Fig. 3 as a total strength within bins as a function of the mass number A of the even-even reference nucleus (i.e., of the $\beta\beta$ mother nucleus). The panels of the figure clearly indicate that the cumulative strength increases with increasing mass number in accordance with the Ikeda $3(N-Z)$ sum rule since the difference $N-Z$ increases with the mass number A and the β^+ strength is always very small compared with the β^- strength. This same information can be directly read from the tenth column of Table I where the computed total GT strength is given. We want to stress here that our calculations obey quite accurately the Ikeda sum rule in all the studied cases.

The projected pn-dQRPA of Refs. [24,25] was recently used to describe low-energy GT strength functions in ^{150}Nd in Ref. [46] by different Skyrme forces. There similar results as in Ref. [34] were obtained for the β^- strength function in the range $0 \leqslant \omega \leqslant 30$ MeV. The studies were extended in Ref. [47] to ^{76}Ge, ^{116}Cd, ^{128}Te, and ^{130}Te, including also ^{150}Nd. The corresponding cumulative strengths were plotted in Fig. 3 of Ref. [47] up to 3 MeV of excitation in the daughter nuclei. In the case of ^{150}Nd, our computed cumulative strength follows closer to the experiment than in Ref. [47]. Also for ^{76}Ge, ^{128}Te, and ^{130}Te our computed cumulative strength is

TABLE III. Gamow-Teller strength summed over 0.5 MeV-wide energy intervals. The excitation energy is always relative to the ground state of the odd-odd daughter nucleus.

n	Parent		Energy bins in MeV											
	Z	A	0.0–0.5	0.5–1.0	1.0–1.5	1.5–2.0	2.0–2.5	2.5–3.0	3.0–3.5	3.5–4.0	4.0–4.5	4.5–5.0	5.0–5.5	5.5–6.0
1	30	70	0.26	0.04	0.07	1.41	0.08	0.05	1.65	0.00	0.11	0.00	0.01	0.14
2	32	76	0.05	0.20	0.16	0.39	0.23	1.12	0.48	0.50	0.05	0.02	0.08	0.71
3	34	80	0.16	0.03	0.34	0.41	0.15	2.28	0.18	0.13	0.16	0.00	1.46	0.41
4	34	82	0.12	0.08	0.26	0.31	0.42	1.11	1.63	0.01	0.03	0.01	1.23	0.71
5	36	86	0.05	0.12	0.74	1.52	0.80	1.14	0.05	0.00	0.00	0.00	0.12	0.35
6	40	94	0.10	0.06	0.03	0.01	0.02	0.02	0.10	0.31	0.74	1.51	0.61	0.52
7	40	96	0.30	0.01	0.06	0.03	0.11	0.05	0.02	0.91	0.16	0.21	0.38	1.32
8	42	100	0.24	0.09	0.20	0.02	0.08	0.02	0.32	0.72	0.11	0.16	1.04	0.77
9	44	104	0.19	0.24	0.11	0.01	0.05	0.04	0.59	0.34	0.25	0.62	0.26	0.83
10	46	110	0.49	0.00	0.13	0.24	0.01	0.29	0.65	0.13	0.16	0.24	0.35	0.63
11	52	128	0.38	0.03	0.01	0.32	0.03	1.80	1.13	0.02	4.80	0.02	0.00	0.00
12	52	130	0.34	0.02	0.00	0.32	0.01	1.63	0.09	1.04	0.00	3.94	0.00	0.00
13	54	134	0.33	0.00	0.05	0.21	0.00	1.71	0.04	0.02	1.51	2.83	0.00	0.00
14	54	136	0.28	0.02	0.00	0.07	0.18	0.01	1.56	0.00	0.00	1.31	0.00	0.00
15	58	142	0.14	0.31	0.18	0.05	0.01	0.00	1.51	0.05	0.00	0.00	1.52	0.37
16	60	148	0.16	0.02	0.05	0.12	0.10	0.03	0.06	0.13	0.52	0.60	0.10	1.11
17	60	150	0.16	0.03	0.16	0.02	0.15	0.07	0.03	0.11	0.15	0.58	0.41	0.06
18	62	154	0.17	0.15	0.13	0.01	0.00	0.21	0.08	0.06	0.12	0.65	0.14	0.18
19	64	160	0.13	0.27	0.07	0.04	0.02	0.27	0.02	0.05	0.11	0.58	0.19	0.22
20	70	176	0.09	0.26	0.45	0.03	0.02	0.04	0.09	0.15	0.07	0.10	0.22	0.22

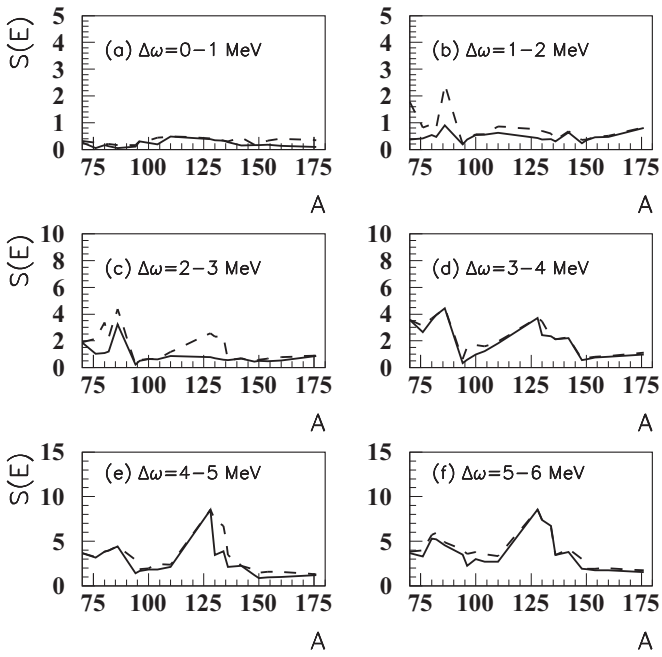

FIG. 3. Cumulative GT strength vs the mass number A summed over energy intervals $E(\omega) = n - (n + 0.5)$ MeV (solid lines) and $E(\omega) = (n + 0.5) - (n + 1)$ MeV (dashed lines) for $n = 0$ (a), $n = 1$ (b), $n = 2$ (c), $n = 3$ (d), $n = 4$ (e), and $n = 5$ (f), given in Table III.

closer to experiment below 2.5 MeV. However, within the bin $2.5 \leqslant \omega \leqslant 3.0$ MeV our computed strength exceeds the measured one as seen also in Figs. 1(a) and Figs. 2(a) and 2(b). Still, even up to $\omega = 8$–10 MeV our computed strength follows the experimental trend reasonably well.

IV. CONCLUSIONS

Concluding, we described the 1^+ Gamow-Teller states in odd-odd deformed nuclei within a consistent proton-neutron deformed QRPA framework, by using a single-particle basis with good angular momentum, provided by the diagonalization of a spherical mean field plus quadrupole-quadupole interaction. This approach gives a consistent description of a deformed nucleus in the laboratory system of coordinates.

The available experimental β^--decay strengths are reasonably described within a schematic pairing plus proton-neutron residual interaction in particle-hole and particle-particle channels. The value $g_{\rm pp} \approx 0.04$ MeV reproduces quite nicely the experimental $2\nu\beta\beta$ half-lives of eight emitters. We predict total Gamow-Teller strengths, $2\nu\beta\beta$ half-lives, and low-lying β^--decay strengths for a number of potential $2\nu\beta\beta$ emitters for comparison with future experimental results.

ACKNOWLEDGMENTS

This work has been partially supported by the Academy of Finland (Suomen Akatemia) under the Finnish Centre of Excellence Programme 2012–2017 (Nuclear and Accelerator Based Programme at JYFL) and the Grants No. PN-II-ID-PCE-2011-3-0092 and No. PN-16420101 of the Romanian National Authority for Scientific Research.

[1] F. T. Avignone III, S. R. Elliott, and J. Engel, Rev. Mod. Phys. **80**, 481 (2008).
[2] J. Maalampi and J. Suhonen, Adv. High Energy Phys. **2013**, 505874 (2013).
[3] J. Suhonen and O. Civitarese, Phys. Rep. **300**, 123 (1998).
[4] A. Escuderos, A. Faessler, V. Rodin, and F. Šimkovic, J. Phys. G: Nucl. Part. Phys. **37**, 125108 (2010).
[5] J. Suhonen and O. Civitarese, J. Phys. G: Nucl. Part. Phys. **39**, 124005 (2012).
[6] R. Sahu, P. C. Srivastava, and V. K. B. Kota, J. Phys. G: Nucl. Part. Phys. **40**, 095107 (2013).
[7] J. Engel, J. Phys. G: Nucl. Part. Phys. **42**, 034017 (2015).
[8] J. Suhonen, Phys. Lett. B **607**, 87 (2005).
[9] D. Frekers, P. Puppe, J. H. Thies, and H. Ejiri, Nucl. Phys. A **916**, 219 (2013).
[10] P. Puppe, D. Frekers, T. Adachi *et al.*, Phys. Rev. C **84**, 051305(R) (2011).
[11] C. J. Guess, T. Adachi, H. Akimune *et al.*, Phys. Rev. C **83**, 064318 (2011).
[12] J. H. Thies, D. Frekers, T. Adachi *et al.*, Phys. Rev. C **86**, 014304 (2012).
[13] J. H. Thies, P. Puppe, T. Adachi *et al.*, Phys. Rev. C **86**, 054323 (2012).
[14] J. H. Thies, T. Adachi, M. Dozono *et al.*, Phys. Rev. C **86**, 044309 (2012).
[15] P. Puppe, A. Lennarz, T. Adachi *et al.*, Phys. Rev. C **86**, 044603 (2012).
[16] J. Barea, J. Kotila, and F. Iachello, Phys. Rev. C **87**, 014315 (2013).
[17] J. Suhonen and O. Civitarese, Nucl. Phys. A **847**, 207 (2010).
[18] J. Suhonen, Nucl. Phys. A **853**, 36 (2011).
[19] J. Menéndez, A. Poves. E. Caurier, and F. Nowacki, Nucl. Phys. A **818**, 139 (2009).
[20] S. Singh, R. Chandra, P. K. Rath, P. K. Raina, and J. G. Hirsch, Eur. Phys. J. A **33**, 375 (2007).
[21] T. R. Rodriguez and G. Martinez-Pinedo, Phys. Rev. Lett. **105**, 252503 (2010).
[22] Z.-C. Gao, Y. Sun, and Y.-S. Chen, Phys. Rev. C **74**, 054303 (2006).
[23] J. Suhonen and O. Civitarese, J. Phys. G: Nucl. Part. Phys. **39**, 085105 (2012).
[24] P. Sarriguren, E. Moya de Guerra, A. Escuderos, and A. C. Carrizo, Nucl. Phys. A **635**, 55 (1998).
[25] P. Sarriguren, E. Moya de Guerra, and A. Escuderos, Nucl. Phys. A **658**, 13 (1999); **691**, 631 (2001).
[26] L. Pacearescu, V. Rodin, F. Simkovic, and A. Faessler, Phys. Rev. C **68**, 064310 (2003).
[27] F. Šimkovic, L. Pacearescu, and A. Faessler, Nucl. Phys. A **733**, 321 (2004).
[28] R. Alvarez-Rodriguez, P. Sarriguren, E. Moya de Guerra, L. Pacearescu, A. Faessler, and F. Šimkovic, Phys. Rev. C **70**, 064309 (2004).
[29] P. Sarriguren, Phys. Rev. C **86**, 034335 (2012).
[30] A. A. Raduta, D. S. Delion, and N. Lo Iudice, Nucl. Phys. A **551**, 93 (1993).

[31] A. A. Raduta, D. S. Delion, and A. Faessler, Phys. Lett. B **312**, 13 (1993).
[32] A. A. Raduta, A. Escuderos, A. Faessler, E. Moya de Guerra, and P. Sarriguren, Phys. Rev. C **69**, 064321 (2004).
[33] D. S. Delion and J. Suhonen, Phys. Rev. C **87**, 024309 (2013).
[34] D. S. Delion and J. Suhonen, Phys. Rev. C **91**, 054329 (2015).
[35] O. Civitarese and J. Suhonen, J. Phys. G: Nucl. Part. Phys. **20**, 1441 (1994).
[36] O. Civitarese and J. Suhonen, Nucl. Phys. A **578**, 62 (1994).
[37] J. Suhonen, *From Nucleons to Nucleus: Concepts of Microscopic Nuclear Theory* (Springer, Berlin, 2007).
[38] J. Dudek, W. Nazarewicz, and T. Werner, Nucl. Phys. A **341**, 253 (1980).
[39] P. Möller and J. R. Nix, Nucl. Phys. A **272**, 502 (1995).
[40] D. S. Delion and J. Suhonen, Eur. Phys. Lett. **107**, 52001 (2014).
[41] A. S. Barabash, AIP Conf. Proc. **1572**, 11 (2013).
[42] E. Caurier, F. Nowacki, and A. Poves, Phys. Lett. B **711**, 62 (2012).
[43] P. Pirinen and J. Suhonen, Phys. Rev. C **91**, 054309 (2015).
[44] F. F. Deppisch and J. Suhonen, Phys. Rev. C **94**, 055501 (2016).
[45] R. Madey, B. S. Flanders, B. D. Anderson *et al.*, Phys. Rev. C **40**, 540 (1989).
[46] D. Navas-Nicolás and P. Sarriguren, Phys. Rev. C **91**, 024317 (2015).
[47] P. Sarriguren, O. Moreno, and E. Moya de Guerra, Adv. High Energy Phys. **2016**, 6391052 (2016).